Ceramics-Silikáty 69 (1), 54-62 (2025)
www.ceramics-silikaty.cz doi: 10.13168/cs.2024.0065

MODULATION OF STRUCTURE AND PROPERTIES IN Li_2O-Al_2O_3-B_2O_3 GLASS-CERAMICS THROUGH TiO_2 AND P_2O_5 ADDITIVES

SIJIA HU*, KUN ZHOU*, HAILEI XIE*, ZIXIN CAO*, SHUWANG DUO*,**, #JIANG SHI*, **

*School of Materials and Energy, Jiangxi Science and Technology Normal University, Nanchang 330013, China
**Jiangxi Province Key Laboratory of Surface Engineering, Jiangxi Science and Technology Normal University, Nanchang 330013, China

#E-mail: whutsj@126.com

Submitted September 27, 2024, accepted October 25, 2024

Keywords: Glass-ceramic, Aluminoborate glass, Transmittance, Scratch resistance, Nucleating agent

Aluminoborate glass is known for its high resistance to crack propagation. However, its relatively low hardness limits its broader application in cover glass technologies. In this study, an Li_2O-Al_2O_3-B_2O_3 (LAB) parent glass was prepared via melt-casting and subjected to a crystallisation treatment at 575 °C for 1 h. The effects of varying the TiO_2/P_2O_5 nucleating agent ratios on the microstructure, visible light transmittance, Vickers hardness, and scratch resistance of both the parent glass and the resulting glass-ceramics were systematically investigated. The experimental results revealed that under identical heat treatment conditions, the $Li(Al_7B_4O_{17})$ crystalline phase was successfully precipitated from the parent glass. When the TiO_2/P_2O_5 ratio was 1, the composite nucleating agent exhibited the strongest ability to promote crystallisation in the glass. The resulting LAB glass-ceramic exhibited well-arranged, densely packed crystalline grains with sizes ranging from 20 to 30 nm. The sample achieved a visible light transmittance of 79.5 %, a hardness of 6.51 GPa, and a CR value of 13.38 N, indicating superior scratch resistance. These properties suggest the potential application of this glass-ceramic in cover glass technologies.

INTRODUCTION

With the rapid advancement of the fifth-generation mobile communication technology (5G), large-screen display technology has emerged as a pivotal element in information interaction and audiovisual experiences. Cover glass, serving as the core component of touch screens, plays a crucial role in determining the durability and overall user experience of devices. Notably, there is an ever-increasing demand for enhanced crack resistance and hardness, highlighting the paramount importance of its performance.

Silicate glass, particularly aluminosilicate glass, meets the primary requirements of most commercial applications. The strength of the glass increases with higher concentrations of Al_2O_3 and SiO_2. However, this also makes the melting and forming processes more challenging, leading to higher manufacturing costs. Aluminoborate glass, a novel glass material where B_2O_3 and Al_2O_3 serve as network formers, does not contain high-melting-point oxides such as SiO_2. The presence of a substantial amount of low-melting-point B_2O_3 significantly lowers the melting temperature compared to silicate glass, making it easier to control during the forming process [1]. Moreover, aluminoborate glass exhibits exceptional crack resistance. The research conducted by Januchta K. et al. [2] revealed that Li_2O-Al_2O_3-B_2O_3 (LAB) glass, after being processed under hot-pressing conditions, demonstrated superior crack resistance (CR) compared to aluminosilicate glass, with a CR value of nearly 31 N. The study attributed this enhanced CR to the transformation of boron (B) and aluminium (Al) into higher coordination states during hot pressing, leading to a denser microstructure. Consequently, aluminoborate glass achieves remarkable CR properties. In summary, compared to silicate glass, the energy required for the transition of B and Al atoms from low to high coordination states in aluminoborate glass is significantly lower than the energy needed for a similar transition in Si atoms. This lower energy threshold allows aluminoborate glass to undergo atomic coordination state changes more readily under hot-pressing conditions - a process that is much more challenging for silicate glass [3, 4]. Therefore, aluminoborate glass is more capable

of achieving a high CR compared to silicate glass. Additionally, aluminoborate glass possesses significant scientific research value due to its high thermal stability, excellent mechanical strength, high transparency, and strong ability to form glass with various oxides. These characteristics suggest a promising future for its application in cover glass materials [5, 6]. However, a critical factor currently limiting the rapid development of the aluminoborate glass system is its relatively low microhardness, which falls significantly short of the widely used aluminosilicate glass cover plates, with microhardness values reaching up to 9.34 GPa [7, 8]. Consequently, enhancing the hardness of aluminoborate glass while maintaining its excellent crack resistance presents a challenging yet crucial issue.

Glass-ceramics are produced by precisely controlling the crystallisation kinetics. This is achieved through subjecting the parent glass to heat treatment at predetermined temperatures, thereby promoting the orderly precipitation of crystalline phases from the glass matrix. In comparison to conventional glassy materials, glass-ceramics have demonstrated superior strength and thermal stability, establishing the crystallisation process as an effective strategy for enhancing the properties of glass. The current research on transparent glass-ceramics primarily focuses on systems composed of MgO-Al_2O_3-SiO_2 (MAS) [9, 10], Li_2O-Al_2O_3-SiO_2 (LAS) [11, 12], and Na_2O-CaO-SiO_2 (NCS) [13, 14]. These compositions have garnered significant attention due to their potential for transparency and enhanced properties. Extensive research has demonstrated that crystallisation can significantly enhance the hardness of silicate glass [15-18]. For aluminoborate glass, Zhang et al. [19] discovered that by doping barium aluminoborate glass with Nb_2O_5 and subjecting it to heat treatment, the glass-ceramic's crack resistance and fracture toughness were markedly improved compared to the parent glass, primarily due to the precipitation of the $BaNb_2O_6$ crystalline phase, although the hardness remained largely unchanged. Xie et al. [6] prepared a glass-ceramic with the composition $11Li_2O$-$30Al_2O_3$-$55B_2O_3$-$2TiO_2$-$2P_2O_5$ using a melt-casting method. The precipitation of the $Li(Al_7B_4O_{17})$ crystalline phase resulted in a significant 40.91 % increase in the Vickers hardness. These studies suggest that crystallisation can similarly enhance the hardness of aluminoborate glass. However, the current research on the crystallisation of aluminoborate glass remains relatively limited, and investigations into its structure and properties have not yet reached the depth and comprehensiveness achieved in silicate glass-ceramic systems.

The quantity, size, morphology of crystalline phases, and the characteristics of the residual phase within the glass are critical factors determining the various properties of glass-ceramics. These factors are closely linked to the composition of the glass and the choice of nucleating agents. Selecting an appropriate nucleating agent is crucial for the crystallisation process and the resulting properties of the glass-ceramic. Commonly used oxide nucleating agents include TiO_2 [19, 20], P_2O_5 [21, 22], and ZrO_2 [23, 24]. TiO_2 is frequently employed as a nucleating agent due to the aggregation effect of Ti^{4+} as a high-field-strength cation, which promotes phase separation and subsequently facilitates crystallisation within the glass. P_2O_5 is effective in promoting phase separation within the glass, reducing both the melting and crystallisation temperatures, and its addition does not lead to coloration, making it suitable for use in aluminoborate glass systems. In contrast, adding ZrO_2 increases the viscosity of the glass system, which is detrimental to glass formation and complicates the preparation process. Therefore, ZrO_2 was not incorporated into the glass system in this study.

To develop glass-ceramic materials that exhibit both high hardness and superior crack resistance, this study focuses on Li_2O-Al_2O_3-B_2O_3 glass-ceramics. By employing composite nucleating agents to enhance the nucleation rate, the research investigates the effects of varying ratios of TiO_2 and P_2O_5 nucleating agents on the structure and properties of both the parent aluminoborate glass and the resulting glass-ceramics.

EXPERIMENTAL

The composition of the glass-ceramic used in this experiment is presented in Table 1. After carefully weighing the raw materials according to the specified proportions, they were ball-milled in a planetary ball mill (QM-3SP2, Nanjing University Instrument Factory, China) at 500 rpm for 6 h to ensure thorough mixing. The resulting mixture was then melted in a lift furnace (SG4-8-17, Wuhan Yahua Electric Furnace Co., Ltd., China) at 1450 °C for 1 h. The molten glass was rapidly poured into a preheated graphite mould to form the desired shape. The parent glass sample was subsequently annealed in a muffle furnace (KSL-1100X-S, Hefei Kejing Material Technology Co., Ltd., China) at 500 °C for 2 h to relieve the thermal stress and then cooled slowly within the furnace. The resulting Li_2O-Al_2O_3-B_2O_3 (LAB) base glasses were designated as Z1, Z2, and Z3, respectively. During the preparation of the glass-ceramic, the annealed glass was cut into thin slices measuring 20 × 10 × 1.6 mm using a diamond wire cutting machine (STX-202A, Shenyang Kejing Material Technology Co., Ltd., China). These slices underwent crystallisation heat treatment at

Table 1. Chemical composition of the glass-ceramics (wt. %)

Sample ID	Li_2O	Al_2O_3	B_2O_3	TiO_2	P_2O_5	TiO_2/P_2O_5
Z1	11	30	55	1	3	0.33
Z2	11	30	55	2	2	1
Z3	11	30	55	3	1	3

575 °C for 2 h in a muffle furnace, followed by cooling to room temperature within the furnace. The crystallised LAB glass-ceramics were designated as Z1-GC, Z2-GC, and Z3-GC. Before testing, the samples were cut and polished to the appropriate dimensions and surface finish required for the tests.

Microstructure and performance characterisation

This study employed differential scanning calorimetry (DSC, HCT-4plus, HENVEN, China) to precisely determine the critical crystallisation temperature points of the LAB glass system. The parent glass sample was finely ground, sieved, and a 10 mg portion was weighed for analysis in a corundum crucible. The heating rate was set at 10 °C·min^{-1}, and the DSC curve was recorded across a temperature range of 25 °C to 1100 °C. For the phase identification, an X-ray diffractometer (XRD-6100, Shimadzu, Japan) was utilised. A nickel filter was employed to purify the copper target Kα-ray source. The XRD testing conditions were set to 40 kV, with a scanning range from 10° to 80°, a step size of 0.02°, and a scanning speed of 5°/min. The data obtained were analysed using MDI Jade 6.5 software. The microstructure of the samples was observed using scanning electron microscopy (SEM, Sigma, Zeiss, Germany). The glass-ceramic samples were subjected to a series of preparatory steps including cutting, polishing, etching with hydrofluoric (HF) acid (5 %) for 60 s, ultrasonic cleaning, and gold sputtering before the SEM observation. The infrared spectrum of the glass-ceramic was determined using a Fourier transform infrared spectrometer (FT-IR, SPECTRUM TWO, Perkin Elmer, USA). The sample was ground and mixed with KBr, then compressed into pellets for analysis, with a testing range of 400-1600 cm^{-1}. The optical transmittance of the samples was measured using a UV-Visible spectrophotometer (UV-Vis, Lambda 35, Perkin Elmer, USA). The polished samples were scanned in the range of 200-800 nm at a speed of 480 nm·min^{-1}. The hardness of the glass-ceramic was evaluated using a Vickers hardness tester (HM-122, AKASHI, Japan). Each sample underwent three independent tests with a load of 200 g and a dwell time of 10 seconds. The crack resistance, as measured by Vickers hardness tester (HM-122, AKASHI, Japan), is defined by the critical load (CR) at which two of four radial cracks appear, indicating a 50 % probability of crack initiation. The CR was determined by performing indentation tests on samples under loads of 2.94 N, 4.9 N, 9.8 N, 19.6 N, 29.4 N, and 39.2 N. Finally, a scratch test was conducted using a multifunctional material surface performance tester (MFT4000, Lanzhou Huahui Instrument Technology Co., Ltd., China). A diamond tip was used to apply a constant load of 21 N along a 5 mm trajectory at a rate of 10 N·s^{-1}. The resulting changes in scratch depth were meticulously recorded.

RESULTS AND DISCUSSION

Figure 1 presents the DSC curve of the parent glass samples at a heating rate of 10 °C·min^{-1}. By analysing two characteristic points - namely, the glass transition temperature (T_g) and the crystallisation peak temperature (T_p) - it can be discerned that when the TiO_2/P_2O_5 ratio is 0.33, the values for T_g and T_p are 531.94 °C and 632.31 °C, respectively. Conversely, at a TiO_2/P_2O_5 ratio of 3, T_g and T_p are slightly elevated at 535.99 °C and 632.61 °C, respectively. However, when the TiO_2/P_2O_5 ratio is 1, the lowest temperatures are observed, with Tg and T_p measuring at 512.99 °C and 620.40 °C, respectively. These findings indicate that as the TiO_2/P_2O_5 ratio increases, both T_g and T_p exhibit a similar trend, initially decreasing before subsequently increasing. This phenomenon can be attributed to the fact that smaller ionic radii correspond to greater field strengths of ions, which diminishes their capacity to provide free oxygen, thereby impairing their ability to disrupt the glass network structure. In the context of TiO_2 and P_2O_5, the field strength of P^{5+} is greater than that of Ti^{4+}. As the TiO_2/P_2O_5 ratio escalates, the network disruption capability of TiO_2 becomes more pronounced, leading to a reduction in glass stability, which favours the crystallisation of the glass. However, as the TiO_2/P_2O_5 ratio continues to increase, the presence of Al_2O_3 may result in P_2O_5 reinforcing the network through its interaction with $(AlO_4)^{5-}$, thereby significantly enhancing the network's integrity and rendering crystallisation more challenging. A comprehensive analysis reveals that at a TiO_2 to P_2O_5 ratio of 1:1, the crystallisation temperature of the glass is at its lowest, indicating that, at this juncture, the composite nucleating agent exerts the most potent promoting effect on crystallisation.

Figure 2 illustrates the XRD patterns of the parent glass and glass-ceramic samples. As observed in Figure 2a, the XRD profile of the LAB parent glass containing varying proportions of TiO_2/P_2O_5 displays a pronounced amorphous halo peak between 20° and

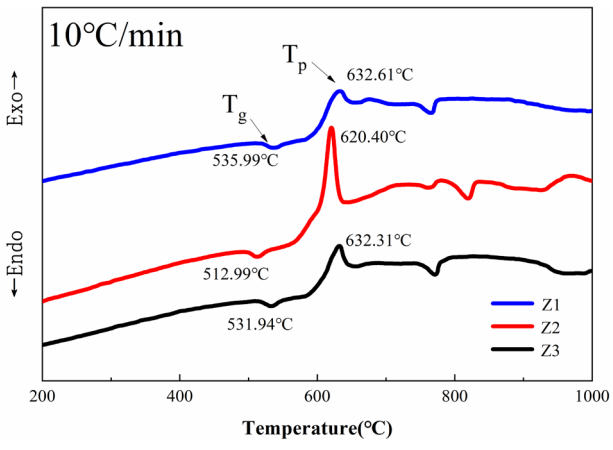

Figure 1. Results of the DSC for the parent glass.

30°, with no sharp diffraction peaks emerging in other angular ranges. This indicates that no crystalline phases have formed in the parent glass produced via the melt-casting method. Figure 2b reveals that the glass-ceramic obtained after heat treatment at 575 °C predominantly crystallises to form the $Li(Al_7B_4O_{17})$ phase (PDF#87-2474). Notably, as the TiO_2/P_2O_5 ratio increases, the intensity of the diffraction peaks initially strengthens before subsequently diminishing. This observation suggests that an increase in the TiO_2/P_2O_5 ratio initially facilitates crystallisation in the glass samples, while further increments hinder this process. This result is in alignment with the findings from the DSC analysis. To further quantify the content of the $Li(Al_7B_4O_{17})$ phase, the phase content and crystallinity results obtained through the Rietveld refinement calculations are presented in Table 2. As indicated in the table, the crystallinity of the glass samples initially increases from 46.4 % to 67.9 % with the increasing TiO_2/P_2O_5 ratios, before declining to 52.1 %. This trend is consistent with the XRD analysis results.

Table 2. XRD Rietveld refinement results of the glass-ceramic samples.

Sample ID	Z1-GC	Z2-GC	Z3-GC
Crystallinity (%)	46.4	67.9	52.1

Figure 3 presents the SEM images of the glass-ceramics. From Figure 3, it is evident that after etching with HF, the crystalline in all three sample groups are clearly exposed. The crystallised glass-ceramics exhibit a significant presence of crystalline phases, with a similar microstructure across the samples. The micrographs reveal a large number of well-organised, uniformly distributed, granular crystals. Based on the XRD patterns shown in Figure 2, these granular crystalline phases can be identified as $Li(Al_7B_4O_{17})$. Furthermore, the introduction of varying TiO_2/P_2O_5 ratios impacts the precipitation of the crystalline phase differently. In Figures 3a and 3c, where the TiO_2/P_2O_5 ratios are 0.33 and 3, respectively, the samples exhibit smaller and more densely packed crystals. When the TiO_2/P_2O_5 ratio is 1, the crystal size is significantly larger, indicating a more pronounced crystal growth process at this ratio. The measured crystal sizes for the Z1-GC, Z2-GC, and Z3-GC samples are 15-25 nm, 20-30 nm, and 10-20 nm, respectively. These findings suggest that variations in the TiO_2/P_2O_5 ratio affect the size of the precipitated crystals, primarily due to the nucleating agent's role in promoting crystallisation. This enhancement in the crystallisation is reflected in both the crystallisation rate and the growth size of the crystalline phase. Specifically, in the borate-aluminosilicate glass system studied in this experiment, a TiO_2/P_2O_5 ratio of 1 not only accelerates the crystallisation rate, but also effectively promotes

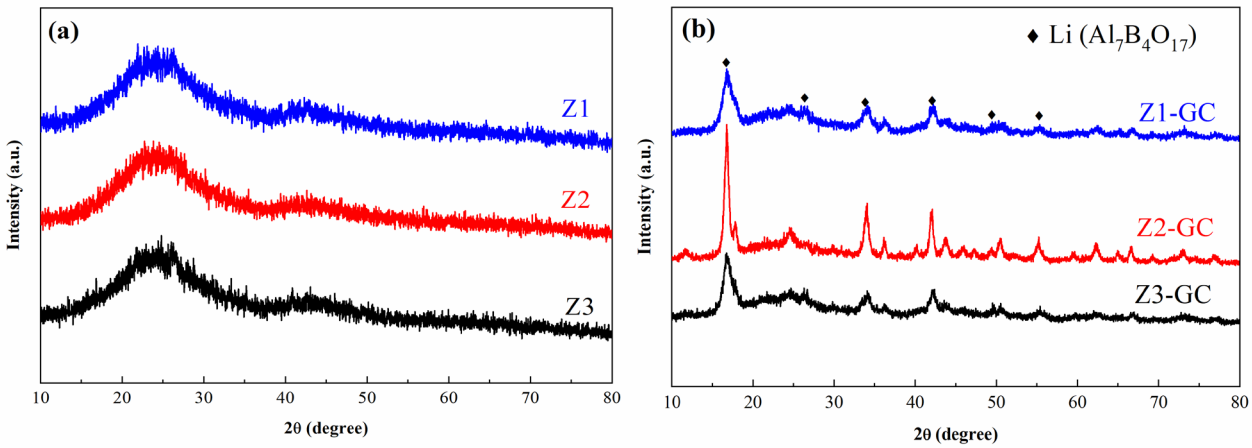

Figure 2. XRD patterns of the (a) parent glass and (b) glass-ceramics.

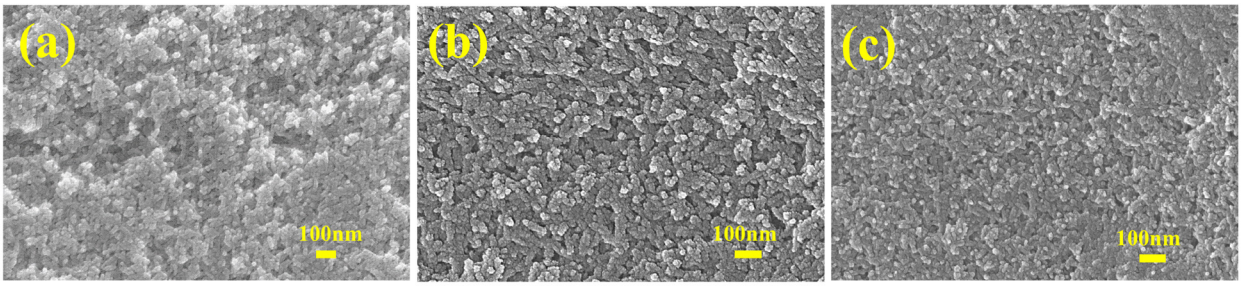

Figure 3. SEM images of the glass-ceramics.

crystal growth. Thus, a TiO_2/P_2O_5 ratio of 1 result in glass-ceramics with the largest precipitated crystal size.

Figure 4a illustrates the FTIR spectrum of the parent glass. The absorption band at 469 cm^{-1} corresponds to the Al-O stretching vibrations in the [AlO_4] units [25, 26]. The band observed at 704 cm^{-1} is attributed to the bending vibrations of the B-O-B bonds within the [BO_3] units, as well as the stretching vibrations of Al-O-B bonds [27, 28]. The absorption band at 784 cm^{-1} is related to the Al-O stretching vibrations in the [AlO4] units [27]. Additionally, the band at 1075 cm^{-1} is likely due to the stretching vibrations of B-O bonds in the [BO_4] units present in the tri-, tetra-, and penta-borate groups [29]. The absorption band observed at 1400 cm^{-1} is associated with the stretching vibrations of the B-O bonds in borate rings ([BO_3]) [30], while the band at 1205 cm^{-1} arises from the stretching vibrations of the triangular [BO_3] units [31, 32]. It is noteworthy that, as the TiO_2/P_2O_5 ratio increases, the intensities of the absorption peaks at 469 cm^{-1} and 704 cm^{-1} exhibit a slight decrease, though the change is not significant. Conversely, the intensity of the absorption peak at 1075 cm^{-1} initially increases and then decreases, indicating that the content of the [BO_4] units increases with the TiO_2/P_2O_5 ratio up to a certain point before subsequently diminishing.

In comparison to the FTIR spectrum of the parent glass, the glass-ceramic samples exhibit additional absorption bands at 542 cm^{-1}, 662 cm^{-1}, and 873 cm^{-1}, which can be attributed to the precipitation of crystalline phases. According to the literature, the absorption band at 542 cm^{-1} is associated with the stretching vibrations of [BO_3] units [27], while the band at 662 cm^{-1} corresponds to the bending vibrations of the O-B-O bonds [33]. The absorption peak at 873 cm^{-1} is attributed to the B-O bond vibrations within the [BO_4] units [34, 35]. Spectral analysis reveals that the intensity of these three absorption peaks increases initially with the rise in the TiO_2/P_2O_5 ratio, followed by a subsequent decrease. This trend suggests that the vibrations of the [BO_3] units first intensify and then weaken. Additionally, considering the changes in the peak intensities at 704 cm^{-1} and 762 cm^{-1}, it can be inferred that the content of [BO_3] units decreases, whereas the content of [AlO4] units increases. Literature sources indicate that the band at 873 cm^{-1} is attributable to the B-O bond vibrations in [BO_4] units, which implies an enhancement in the vibrations of [BO_4] units. The increased intensity of the absorption peak at 1087 cm^{-1} further corroborates the increased content of [BO_4] units in the Z2 sample.

Figure 5 presents the transmittance curves of LAB glass-ceramics containing varying ratios of TiO_2/P_2O_5. From this graph, it is evident that at 550 nm, the transmittance values for the Z1-GC, Z2-GC, and Z3-GC glass-ceramic samples are 87.5 %, 79.5 %, and 86.44 %, respectively, with Z2-GC exhibiting the lowest transmittance. The analysis of the SEM images of the glass-ceramics reveals that when the TiO_2/P_2O_5 ratio is set at 1, Z2-GC exhibits the largest grain size

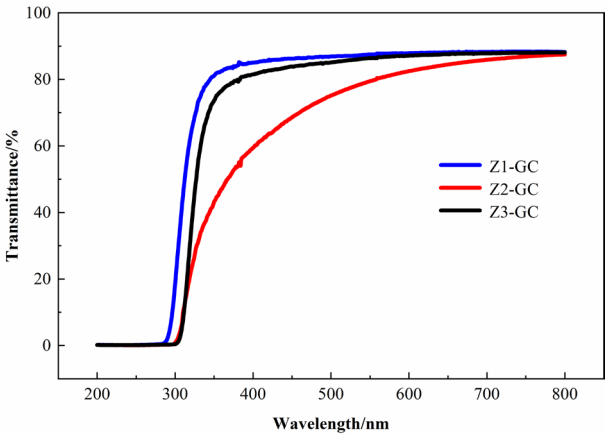

Figure 5. The transmittance curves of the LAB glass-ceramics.

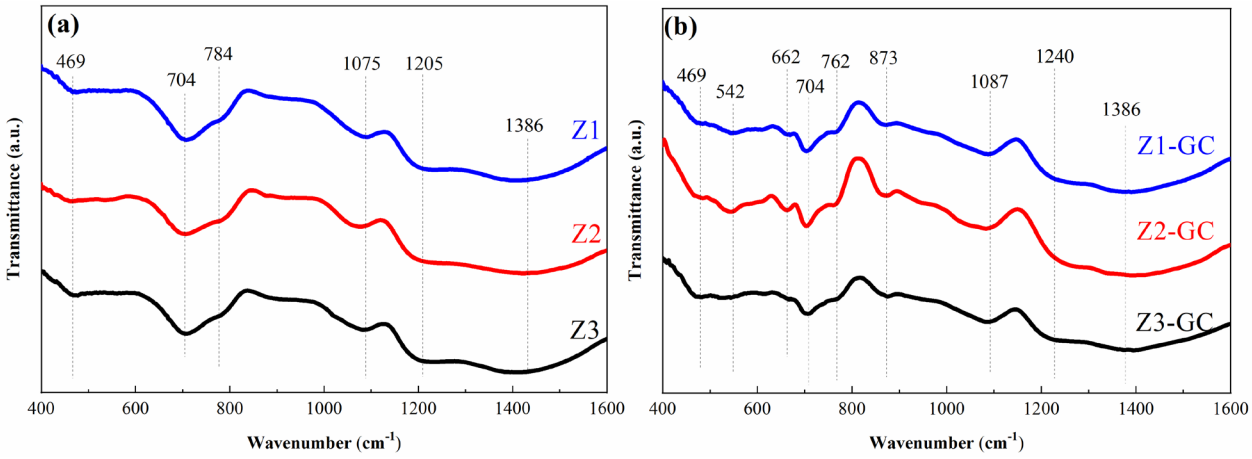

a) parent glass b) glass-ceramics

Figure 4. FT-IR spectra of the (a) parent glass and (b) glass-ceramics.

of the precipitated crystalline phases, characterised by a dense distribution. According to the Mie theory, larger grain sizes result in the more pronounced scattering and absorption of visible light. Consequently, when visible light strikes the surface of the glass and attempts to penetrate its interior, the losses are intensified, leading to a lower visible light transmittance in Z2-GC glass. Conversely, the grain sizes in the Z1-GC and Z3-GC samples are relatively smaller compared to those in Z2-GC, thus resulting in a correspondingly higher visible light transmittance.

Figure 6 displays the hardness test results for both the parent glass and the glass-ceramics. As evident from the figure, variations in the TiO_2/P_2O_5 ratio have minimal impact on the hardness of the LAB parent glass, with the hardness values consistently around 4.6 GPa. However, upon subjecting this glass system to heat treatment at 575 °C for crystallisation, there is a significant enhancement in the hardness of the glass. This improvement can be attributed primarily to the role of TiO_2 and P_2O_5 as nucleating agents. The presence of these nucleating agents facilitates the transformation of the parent glass into crystalline phases during heat treatment. The precipitated crystalline phases typically exhibit higher density compared to the amorphous phase, which contributes to the increased hardness of the glass.

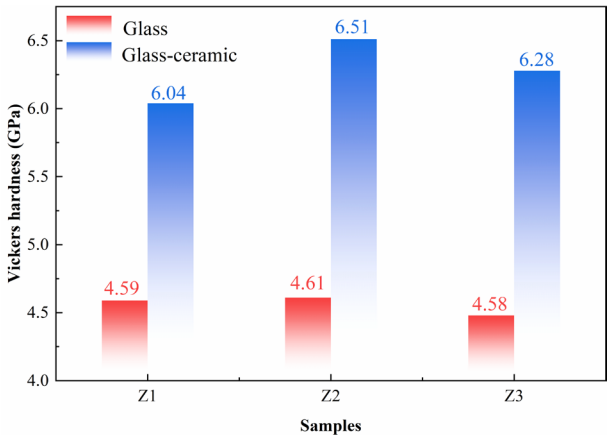

Figure 6. The hardness test results of the parent glass and glass-ceramics.

Furthermore, the presence of crystalline phases helps to limit and obstruct shear flow and local densification around indentations caused by hard object penetration, thereby enhancing the hardness of the glass-ceramics. Additionally, the microhardness of the glass-ceramics initially increases and then decreases with the rising TiO_2/P_2O_5 ratio, reaching its peak value of 6.51 GPa in the Z2-GC sample. This peak is largely due to the fact that when the TiO_2/P_2O_5 ratio is 1, the crystallinity of the sample is at its highest, resulting in the most effective improvement in microhardness due to the precipitated crystalline phases.

Figure 7 presents the CR test results for the samples, along with the fitted curve, which was generated using the function $y = A_2 + (A_1 - A_2) / [1 + (x/x_0)p]$, as referenced from the method employed by R. Limbach [36]. From Figure 7c, it is apparent that the CR values of the parent glasses with different TiO_2/P_2O_5 ratios are relatively similar, all within the range of 21 to 25 N. However, the CR value of Z2 (21.68 N) is slightly lower than those of Z1 and Z3. This observation aligns with the previous analysis, where it was noted that the content of $[BO_4]$ units in the parent glass first increases and then decreases as the TiO_2/P_2O_5 ratio increases, with the Z2 sample containing the highest amount of $[BO_4]$ units. Studies have shown that the crack resistance increases with the rise in $[BO_3]$ units [2]. The reason for this is that B atoms in low coordination states can absorb the residual stress generated during indentation by transitioning to higher coordination states, thereby preventing crack formation within the glass. Consequently, the greater quantity of $[BO_4]$ units in the Z2 sample results in a lower CR value. For the glass-ceramic samples, it is evident that the CR values decrease significantly after crystallisation compared to their corresponding parent glasses, indicating that the precipitation of crystalline phases within the glass reduces its crack resistance. Notably, the Z2-GC sample exhibits the lowest CR value (13.38 N) among all the samples. According to the XRD results presented in Table 2, the Z2-GC sample has the highest degree of crystallinity (67.9 %) among the tested samples, suggesting that the higher the crystallinity

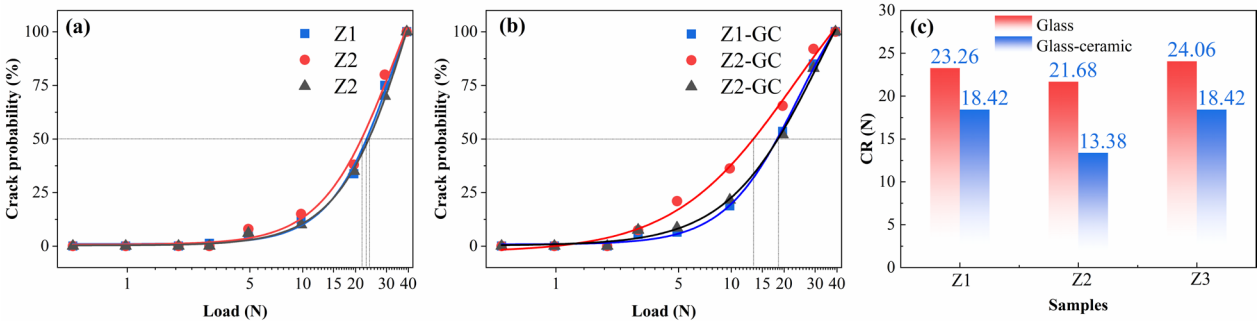

Figure 7. The CR test results for the samples, (a) parent glass, (b) glass-ceramic, and (c) CR values of the samples.

of the glass-ceramic, the lower its crack resistance. In fact, for glass-ceramics, the coordination numbers of B and Al in the precipitated $Li(Al_7B_4O_{17})$ crystalline phase are fixed, meaning that they cannot increase their coordination numbers in response to external forces to enhance crack resistance, unlike the residual amorphous phase. Therefore, the greater the amount of precipitated crystalline phases in the glass, the lower the CR value of the glass-ceramic.

Figure 8 illustrates the results of the scratch tests conducted on the samples. It is evident from this figure that variations in the TiO_2/P_2O_5 ratio have minimal impact on the scratch width of the LAB parent glass, which consistently measures around 117 μm. In contrast, the scratch widths of the glass-ceramics with differing TiO_2/P_2O_5 ratios are notably reduced compared to the parent glass, indicating a significant enhancement in scratch resistance following crystallisation. This improvement in scratch resistance can be attributed to the effective suppression of crack propagation by the precipitated crystalline phases, which also contributes to the overall increase in glass hardness. Furthermore, when comparing the scratch widths of the different TiO_2/P_2O_5 glass-ceramics, it is noteworthy that the Z2-GC, with a TiO_2/P_2O_5 ratio of 1, exhibits a significantly smaller scratch width of 104.41 μm, in contrast to the Z1-GC and Z3-GC samples. This finding is consistent with the hardness test results presented in Figure 6, reinforcing the notion that the Z2-GC exhibits the best scratch resistance. Moreover, integrating the insights from the SEM and XRD analyses reveals that the high scratch resistance of this glass-ceramic can be attributed to the substantial presence of dense, nanoscale grains formed within the matrix, which effectively obstructs the formation and propagation of cracks.

CONCLUSION

In this study, the structure of aluminosilicate glasAfter crystallisation at 575 °C for 1 h, Li_2O-Al_2O_3-B_2O_3 parent glasses containing varying ratios of TiO2/P_2O_5 precipitate the granular $Li(Al_7B_4O_{17})$ crystalline phase. Among them, the composite nucleating agent with a TiO_2/P_2O_5 ratio of 1 demonstrates the most effective promotion of crystallisation, leading to the formation of tightly packed and relatively larger crystalline grains. Following heat treatment, the hardness and scratch resistance of glass-ceramics with different ratios of the nucleating agent are significantly improved compared to the parent glass. When the TiO_2/P_2O_5 ratio is 0.33 and 3, the precipitated crystalline phases measure 15-25 nm and 10-20 nm, respectively, whereas at a ratio of 1, the crystalline phase size increases to 30-40 nm. At this ratio, the visible light transmittance of the glass-ceramic is slightly lower than that of other samples. Specifically, the Li_2O-Al_2O_3-B_2O_3 glass-ceramic with a TiO_2/P_2O_5 ratio of 1 exhibits a hardness of 6.51 GPa and a crack resistance (CR) value of 13.38 N. This composition achieves the best scratch resistance while maintaining 79.5 % transmittance in the visible light region, indicating its potential for application in cover glass technologies.

Acknowledgements

This work is supported by Jiangxi Provincial Natural Science Foundation (No. 20242BAB20170), Jiangxi Province Key Laboratory of Surface Engineering (No. 2024SSY05071), and the Doctoral Research Initiation Fund of Jiangxi Science and Technology Normal University (No. 2021BSQD28).

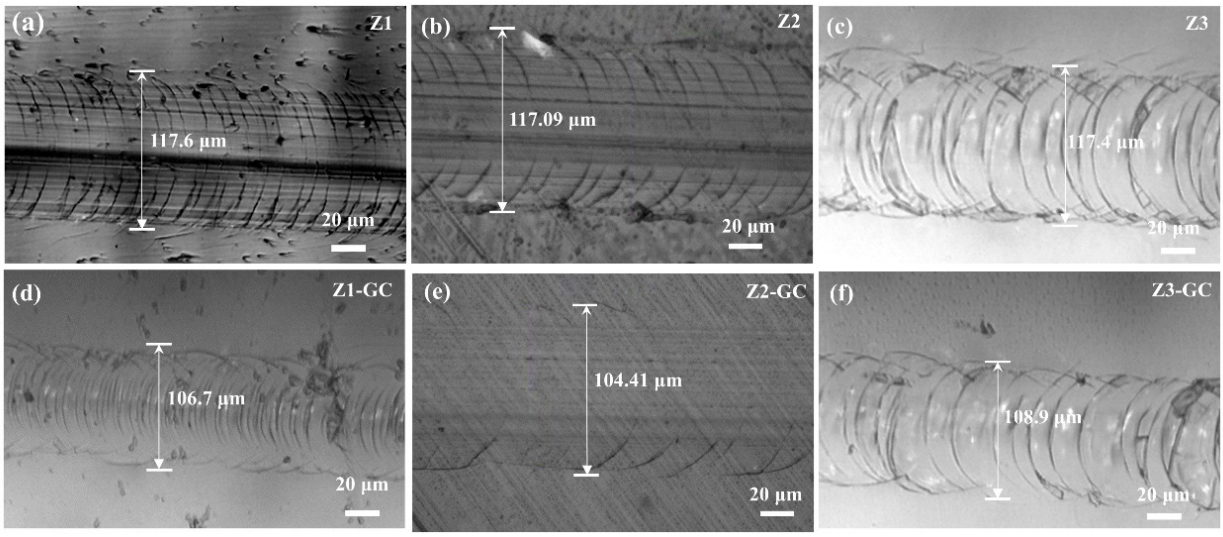

Figure 8. Results of the scratch tests for the various samples: (a)-(c) corresponding to the parent glasses Z1-Z3, and (d)-(f) representing the glass-ceramics Z1-GC to Z3-GC.

REFERENCES

1. Fernandes H.R., Kapoor S., Patel Y., Ngai K., Levin K., Germanov Y., Krishtopa L., Kroeker S., Goel A. (2018): Composition-structure-property relationships in Li_2O-Al_2O_3-B_2O_3 glasses. *Journal of Non-Crystalline Solids, 502*, 142-151. doi: 10.1016/j.jnoncrysol.2018.08.005
2. Januchta K., Youngman R.E., Goel A., Bauchy M., Logunov S.L., Rzoska S.J., Bockowski M., Jensen L.R., Smedskjaer M.M. (2017): Discovery of Ultra-Crack-Resistant Oxide Glasses with Adaptive Networks. *Chemistry of Materials, 29*, 5865-5876. doi: 10.1021/acs.chemmater.7b00921
3. Kapoor S., Wondraczek L., Smedskjaer M.M. (2017): Pressure-Induced Densification of Oxide Glasses at the Glass Transition. *Frontiers in Materials, 4*. doi: 10.3389/fmats.2017.00001
4. Bechgaard T.K., Fuglsang S.D., Pedersen R.H., Tjell A.Ø., Østergaard M.B., Youngman R.E., Mauro J.C., Rzoska S.J., Bockowski M., Smedskjaer M.M.et al (2014): Composition-Structure-Property Relations of Compressed Borosilicate Glasses. *Physical Review Applied, 2*, 24006. doi: 10.1103/PhysRevApplied.2.024006
5. Srinivas B., Bhogi A., Naresh P., Hameed A., Chary M.N., Shareefuddin M. (2022): Effect of SrO and TeO_2 on the physical and spectral properties of strontium tellurite boro-titanate glasses doped with Cu^{2+} ions. *Journal of Non-Crystalline Solids, 575*, 121218. doi: 10.1016/j.jnoncrysol.2021.121218
6. Xie H., Zhou K., Hu S., Fu J., Duo S., Shi J. (2024): Enhancement of damage resistance of transparent Li_2O-Al_2O_3-B_2O_3 glass by crystallization. *Journal of Non-Crystalline Solids, 631*, 122911. doi: 10.1016/j.jnoncrysol.2024.122911
7. Chen L., Sun T., Hao Z., Xie J., Zhang J., Han J., Wang M., Cui X., Liang X. (2022): Ultrahigh hardness Li_2O-MgO-Al_2O_3-SiO_2 glass-ceramics containing multiphase nanocrystals. *Journal of the American Ceramic Society, 105*, 7614-7624. doi: 10.1111/jace.18689
8. Zhang T., Zhang Z., Han J., Wang J., Liu C., Ruan J. (2022): The structure and properties of chemical strengthened transparent lithium disilicate glass ceramics with various P_2O_5 contents. *Journal of Non-Crystalline Solids, 588,* 121626. doi: 10.1016/j.jnoncrysol.2022.121626
9. Huang J., Zhang J., Yu Y., Bai H., Zhang Z., Huang Y. (2022): Transparent MgO-Al_2O_3-SiO_2 glass-ceramics prepared with ZrO2 and SnO2 as nucleating agents. *Journal of Non-Crystalline Solids, 588*, 121585. doi: 10.1016/j.jnoncrysol.2022.121585
10. Sant Ana Gallo L., Célarié F., Bettini J., Rodrigues A.C.M., Rouxel T., Zanotto E.D. (2022): Fracture toughness and hardness of transparent MgO-Al_2O_3-SiO_2 glass-ceramics. *Ceramics International, 48*, 9906-9917. doi: 10.1016/j.ceramint.2021.12.195
11. Zheng W., Li C., Yuan J., Tian P., Teng F., Wang W., Peng Z., Wang W. (2022): The Crystallization and Fracture Toughness of Transparent Glass-ceramics with Various Al_2O_3 Additions for Mobile Devices. *Journal of Wuhan University of Technology-Mater. Sci. Ed., 37*, 378-384. doi: 10.1007/s11595-022-2542-y
12. Zhang X., Wang J., Han J. (2023): Crystallization kinetics, structural and mechanical properties of transparent lithium aluminosilicate glass-ceramics. J*ournal of Non-Crystalline Solids, 603*, 122113. doi: 10.1016/j.jnoncrysol.2022.122113
13. Chen B., Han N., Cao X., Guo Y., Liu C. (2021): Microstructure and crystallization properties of Na_2O-CaO-SiO_2 glass system with different ZrO_2 content. *Journal of Non-Crystalline Solids, 573,* 121137. doi: 10.1016/j.jnoncrysol.2021.121137
14. Zhou Z., Tong J., Liang H., Luo Z., Lu A. (2024): Preparation and improved luminescent properties of Tb^{3+}/Yb^{3+} co-doped Na_2O-CaO-SiO_2-Al_2O_3-ZnO-CaF_2 transparent glass-ceramics. *Ceramics International, 50*, 10067-10078. doi: 10.1016/j.ceramint.2023.12.317
15. Bao Z., Wang S., Miao L., Xu Y., Cheng Z., Wang X. (2024): Preparation, properties and formation mechanism of transparent anorthite-based glass-ceramic glaze with high hardness. *Ceramics International, 50*, 26182-26192. doi: 10.1016/j.ceramint.2024.04.359
16. She W., Xu W., Yang T., Cao S., Wang J., Han J. (2023): Microstructure and crystallization behavior of Na_2O-Al_2O_3-SiO_2 glass-ceramics with MgO additions. *Ceramics International, 49,* 22644-22653. doi: 10.1016/j.ceramint.2023.05.012
17 Sun D., Zhang Q., Liu P., Jensen L.R., Wang D., Smedskjaer M.M. (2023): Balancing fracture toughness and transparency in barium titanosilicate glass-ceramics. *Ceramics International, 49,* 17479-17487. doi: 10.1016/j.ceramint.2023.02.115
18 Li W., Wang X., Chen H., Zhang X., Hu L., Chen S. (2023): Influence of fluorine content on crystallization and mechanical properties of SiO_2-Li_2O glass-ceramics. *Ceramics International, 49*, 29123-29132. doi: 10.1016/j.ceramint.2023.06.189
19 Son S., Kim K. (2023): Effect of TiO2 content on crystallization behavior of CaO-Al_2O_3-SiO_2-ZnO glass-ceramic glaze. *Ceramics International, 49,* 13677-13686. doi: 10.1016/j.ceramint.2022.12.245
20 Luo Y., Wang F., Liao Q., Liu L., Wang Y., Zhou J., Xu Y., Zhu H., Gu Y. (2021): Effect of TiO2 on crystallization kinetics, microstructure and properties of building glass-ceramics based on granite tailings. *Journal of Non-Crystalline Solids, 572*, 121092. doi: 10.1016/j.jnoncrysol.2021.121092
21 Zheng W., Zhang H., Wang Q., Yuan J., Tian P. (2024): Effect of P2O5 on nucleation, crystallization and mechanical properties of Y_2O_3-Al_2O_3-SiO_2 glasses. *Ceramics International, 50*, 13467-13477. doi: 10.1016/j.ceramint.2024.01.259
22 Li J., Wang M., Lu P. (2021): Nucleating role of P_2O_5 in nepheline-based transparent glass-ceramics. *Journal of the American Ceramic Society, 104*, 5614-5624. doi: 10.1111/jace.17954
23 Zhu W., Guo S., Zou H., Zu G., Han Y., Ran X. (2022): Effect of ZrO_2 on crystallization behavior and mechanical property of Dy_2O_3-Al_2O_3-SiO_2 glasses. *Ceramics International, 48*, 22468-22478. doi: 10.1016/j.ceramint.2022.04.264
24 Shearer A., Montazerian M., Deng B., Sly J.J., Mauro J.C. (2024): Zirconia-containing glass-ceramics: From nucleating agent to primary crystalline phase. *International Journal of Ceramic Engineering & Science, 6*, e10200. doi: 10.1002/ces2.10200
25 Pernice P., Esposito S., Aronne A., Sigaev V.N. (1999): Structure and crystallization behavior of glasses in the BaO-B_2O_3-Al_2O_3 system. *Journal of Non-Crystalline Solids, 258,* 1-10. doi: 10.1016/S0022-3093(99)00554-2
26 Chryssikos G.D., Bitsis M.S., Kapoutsis J.A., Kamitsos E.I. (1997): Vibrational investigation of lithium metaborate-

metaaluminate glasses and crystals. J*ournal of Non-Crystalline Solids, 217*, 278-290. doi: 10.1016/S0022-3093(97)00224-X

27 Maia L.J.Q., Faria Filho F.M. (2020) 2 - Amorphous and crystalline borate nanocompounds doped with europium ions. In: Pires Kassab L.R., Ribeiro S.J.L., Rangel-Rojo R. (eds) *Nanocomposites for Photonic and Electronic Applications.* Elsevier, pp 31-44. doi: 10.1016/B978-0-12-818396-0.00002-9

28 Wong P.S., Wan M.H., Hussin R., Lintang H.O., Endud S. (2014): Structural and luminescence studies of europium ions in lithium aluminium borophosphate glasses. *Journal of Rare Earths, 32,* 585-592. doi: 10.1016/S1002-0721(14)60112-5

29 Abo-Naf S.M., El Batal F.H., Azooz M.A. (2003): Characterization of some glasses in the system SiO_2, $Na_2O{\cdot}RO$ by infrared spectroscopy. *Materials Chemistry and Physics, 77*, 846-852. doi: 10.1016/S0254-0584(02)00215-8

30 Doweidar H., Saddeek Y.B. (2009): FTIR and ultrasonic investigations on modified bismuth borate glasses. *Journal of Non-Crystalline Solids, 355*, 348-354. doi: 10.1016/j.jnoncrysol.2008.12.008

31 Kaur P., Kaur S., Singh G.P., Singh D.P. (2014): Cerium and samarium codoped lithium aluminoborate glasses for white light emitting devices. *Journal of Alloys and Compounds, 588*, 394-398. doi: 10.1016/j.jallcom.2013.10.181

32 Kaur P., Singh G.P., Kaur S., Singh D.P. (2012): Modifier role of cerium in lithium aluminium borate glasses. *Journal of Molecular Structure, 1020*, 83-87. doi: 10.1016/j.molstruc.2012.03.053

33 Motke S.G., Yawale S.P., Yawale S.S. (2002): Infrared spectra of zinc doped lead borate glasses. *Bulletin of Materials Science, 25*, 75-78. doi: 10.1007/BF02704599

34 Hari Babu B., Ravi Kanth Kumar V.V. (2016): Warm white light generation in γ-irradiated Dy^{3+}, Eu^{3+} codoped sodium aluminoborate glasses. *Journal of Luminescence, 169*, 16-23. doi: 10.1016/j.jlumin.2015.08.058

35 Mishra L., Sharma A., Vishwakarma A.K., Jha K., Jayasimhadri M., Ratnam B.V., Jang K., Rao A.S., Sinha R.K. (2016): White light emission and color tunability of dysprosium doped barium silicate glasses. *Journal of Luminescence, 169*, 121-127. doi: 10.1016/j.jlumin.2015.08.063

36 Limbach R., Winterstein-Beckmann A., Dellith J., Möncke D., Wondraczek L. (2015): Plasticity, crack initiation and defect resistance in alkali-borosilicate glasses: From normal to anomalous behavior. *Journal of Non-Crystalline Solids, 417-418*, 15-27. doi: 10.1016/j.jnoncrysol.2015.02.019